ELSEVIER

Journal of Fluids and Structures 19 (2004) 917–932

JOURNAL OF FLUIDS AND STRUCTURES

www.elsevier.nl/locate/jnlabr/yjfls

Feedback control of rotating disk flutter in an enclosure

X.Y. Huang*, X. Wang, F.F. Yap

Center for Mechanics of Micro-Systems, School of Mechanical & Production Engineering, Nanyang Technological University, Nanyang Avenue, Singapore 639798, Singapore

Received 15 September 2002; accepted 27 April 2004

Available online 12 August 2004

Abstract

This paper presents a feedback control technique applied to flutter of a rotating disk in an enclosure. Rotating disk flutter is an aeroelastic instability induced by the coupling of the disk and the air around the disk. The flutter may occur at high rotation speed and the disk will then vibrate with large amplitude. The control system consists of a sensor to pick up the disk vibrations, and the signals are processed to generate a pressure disturbance in the air inside the enclosure. The instability of the rotating disk is initially analyzed and the disk flutter is observed by calculating the eigenvalues of the disk-enclosure system. The feedback control mechanism is then introduced and the control performance is evaluated based on the control effect on the imaginary parts of the eigenvalues. It is demonstrated that, with a proper combination of the control gain and the phase shift, the feedback control can suppress the disk flutter. The stability map shows that the controller has a large operation region and is therefore robust.

1. Introduction

The stability of rotating disks has recently become an important research topic owing to its applications related to the high capacity and high performance data storage devices, such as hard disk drives for computers. Disks rotating at high speed may be unstable due to coupling with the surrounding air flow, which is called flutter. Disk flutter has been a concern to the data storage industries in order to develop high speed hard disk drives. The disk flutter is a kind of aeroelastic instability, and research on this topic has been related to circular saws [see, for example, Chonan et al. (1985)]. D'Angelo and Mote (1993b) conducted an experiment on thin disks in an enclosure with different air densities. They observed the flutter occurring in (0, 3) mode for a disk rotating at speed about 3500 rpm. They also reported that the flutter speed would increase with a decrease of the air density and confirmed that the flutter was induced by the aerodynamic coupling of the air to the rotating disk. Renshaw et al. (1994) presented an analytical study on the flutter of a rotating disk by taking into account the air coupling and examining the eigenvalues of the whole disk systems. In their modelling, however, the aerodynamic loading on the disk was only the acoustic pressure induced by disk vibrations; no flutter was reported directly from their analysis. Other analytical studies (Hosaka and Crandall, 1992; Yasuda et al., 1992; Chonan et al., 1992; Huang and Mote, 1995; Renshaw, 1998) were conducted focusing on the rotating disks close to rigid surfaces, which are associated with floppy disks used in personal computers. Lubrication theory was employed to model the thin air layers between the disks and casings. In the analytical modelling of disk flutter, the key issue is the coupling of the air dynamics with the disk structure. This has been discussed by Kim et al. (2000) and Hansen et al. (2001), and different models for aerodynamic loading were examined.

*Corresponding author. Tel.: +65-790-4448.
E-mail address: mxhuang@ntu.edu.sg (X.Y. Huang).

0889-9746/$ - see front matter © 2004 Elsevier Ltd. All rights reserved.
doi:10.1016/j.jfluidstructs.2004.04.015

Nomenclature

a	speed of sound
$A(r,\theta)$	actuating surface
$[\mathbf{B}]$	$(M_0+1)\times(M_0+1)$ matrix associated with free vibration of rotating disk
c_m	coefficients for series expansion of w
$[\mathbf{c}]$	$=[\,c_0 \quad c_1 \quad \cdots \quad c_{M_0}\,]^{\mathrm{T}}$
C	nondimensional damping coefficient
C_d	damping coefficient in aerodynamic loading
d_k^a	coefficient of Bessel series for ϕ_a
d_k^c	coefficient of Bessel series for ϕ_c
D	flexural stiffness
E	Young's modulus
G	gain of the feedback control
h	thickness of the disk
m	integers for numbers of nodal circles
M	Mach number at the disk outer edge
M_0	integer of maximum m for the simulation
n	integers for numbers of nodal diameters
$[\mathbf{P}^a]$	$(M_0+1)\times(M_0+1)$ matrix associated with acoustic force
$[\mathbf{P}^c]$	$(M_0+1)\times(M_0+1)$ matrix associated with control force
$[\mathbf{P}^f]$	$(M_0+1)\times(M_0+1)$ matrix associated with aerodynamic force
$\boldsymbol{q}_a$	acoustic loading on disk
$\boldsymbol{q}_c$	control-generated loading on disk
$\boldsymbol{q}_f$	aerodynamic loading on disk
r	r-component in cylindrical coordinate system
r_a	radius of the actuator
r_e	radius of the enclosure
r_i	radius of the clamping collar
r_o	radius of the disk
r_s	r-location of the sensor
t	time
w	transverse displacement of the disk
z	z-component in cylindrical coordinate system
z_e	distance from the upper surface of enclosure to the disk

Greek letters

ε	$D/(\rho_d r_o^4 h\Omega^2)$
θ	θ component of the cylindrical coordinate system
θ_s	θ_s component of the cylindrical coordinate
κ	r_i/r_o
λ	eigenvalue
Λ	mass ratio $\rho_a r_o/\rho_d h$
ν	Poisson ratio of disk
ρ_a	density of air
ρ_d	density of disk
ϕ_a	velocity potential associated with acoustic loading
ϕ_c	velocity potential associated with control generated loading
Ω	rotational speed of disk
Ω_d	rotational speed of damping force in aerodynamic loading

Feedback control techniques have been applied to aerofoil flutter (Huang, 1987), unsteady flows (Huang and Weaver, 1991) and the squeal of train wheels (Heckl et al., 2000). A control technique is proposed in the present study of rotating disk flutter, in which the disk vibration signals are detected and processed to generate pressure perturbations inside the

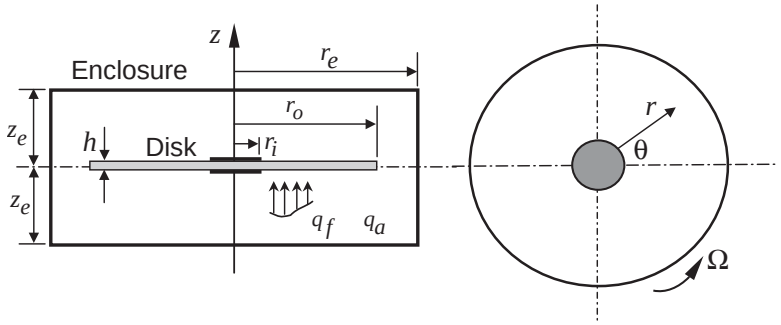

Fig. 1. The geometry of the disk and cylindrical enclosure.

disk enclosure in such way that the original coupling will be altered and the flutter will therefore be suppressed. In order to demonstrate the performance of the feedback control, we simulate the disk-enclosure stability using a viscous damping model (Kim et al., 2000; Hansen et al., 2001) for the aerodynamic loading which will be zero if the disk does not rotate, and considering the acoustic loading as a separate term which always exists as long as the disk is in air or other gases. The controlled acoustic force is an addition to the existing acoustic loading.

2. Fundamental equations

We consider a thin disk rotating inside a cylindrical enclosure which has radius r_e and height $2z_e$, as shown in Fig. 1. The disk has a uniform thickness h and outer radius r_o. It is clamped in the center to a radius r_i. The Young's modulus, Poisson ratio and the density of the disk are, respectively, E, v and ρ_d. The material damping of the disk is assumed to be negligible.[1] The disk rotates at a constant angular speed Ω. The density of the air inside the enclosure is ρ_a. A stationary coordinate system (r,θ,z) is used in the following modelling.

The rotating disk with small transverse motions is modelled following the work by Renshaw et al. (1994), but it is modified by adding an aerodynamic loading and an additional acoustic loading introduced by a feedback actuator. The disk experiences an aerodynamic force $q_f(r,\theta,t)$ arising from the air-flow due to the disk rotation, and an acoustic force $q_a(r,\theta,t)$ arising from the acoustic pressure induced in the enclosure by the disk vibrations; $q_f(r,\theta,t)$ will be zero if the disk does not rotate, while $q_a(r,\theta,t)$ will always be there as long as the disk vibrates in air. The governing equation for the vibration of the disk can be written as

$$\rho h\left(\frac{\partial^2 w}{\partial t^2}+2\Omega\frac{\partial^2 w}{\partial t\partial\theta}+\Omega^2\frac{\partial^2 w}{\partial\theta^2}\right)+D\nabla^4 w-h\left[\frac{1}{r}\frac{\partial}{\partial r}\left(r\sigma_r\frac{\partial w}{\partial r}\right)+\frac{1}{r^2}\frac{\partial}{\partial\theta}\left(\sigma_\theta\frac{\partial w}{\partial\theta}\right)\right]=q_f(r,\theta,t)+q_a(r,\theta,t), \tag{1}$$

where $w(r,\theta,t)$ is the transverse deformation of the disk, $D=Eh^3/12(1-v^2)$ is the flexural stiffness of the disk, $\nabla^4=\left(\frac{\partial^2}{\partial r^2}+\frac{\partial}{r\partial r}+\frac{\partial^2}{r^2\partial\theta^2}\right)^2$ is the biharmonic differential operator, σ_r and σ_θ are, respectively, radial and hoop membrane stresses, which are expressed as follows:

$$\sigma_r=\rho_d r_o^2\Omega^2\left[b_0\left(\frac{r_o}{r}\right)^2+b_1-\frac{3+v}{8}\left(\frac{r}{r_o}\right)^2\right],\quad \sigma_\theta=\rho_d r_o^2\Omega^2\left[-b_0\left(\frac{r_o}{r}\right)^2+b_1-\frac{1+3v}{8}\left(\frac{r}{r_o}\right)^2\right];$$

$$b_0=\frac{(1-v)(r_i/r_o)^2[(3+v)-(1+v)(r_i/r_o)^2]}{8[(1+v)+(1-v)(r_i/r_o)^2]},\quad b_1=\frac{(1+v)[(3+v)+(1-v)(r_i/r_o)^4]}{8[(1+v)+(1-v)(r_i/r_o)^2]}.$$

The disk is clamped by a collar ($r=r_i$), where the displacement w and its slope must be zero, and the boundary conditions are

$$w|_{r=r_i}=0,\quad \left.\frac{\partial w}{\partial r}\right|_{r=r_i}=0. \tag{2}$$

[1] The material damping can be evaluated by considering Young's modulus to be a complex number, and we found that for a steel disk it increased the flutter speed by about 5%.

The disk is free at its rim ($r=r_o$), where the bending moment and shear force must be zero, and the boundary conditions are

$$\left[\frac{\partial^2 w}{\partial r^2}+v\left(\frac{1}{r}\frac{\partial w}{\partial r}+\frac{1}{r^2}\frac{\partial^2 w}{\partial \theta^2}\right)\right]_{r=r_o}=0, \quad \left[\frac{\partial}{\partial r}(\nabla^2 w)+\frac{(1-v)}{r^2}\frac{\partial^2}{\partial \theta^2}\left(\frac{\partial w}{\partial r}-\frac{w}{r}\right)\right]_{r=r_o}=0. \tag{3}$$

The empirical model of aerodynamic loading proposed by Kim et al. (2000) is employed in the present study for the aerodynamic force $q_f(r,\theta,t)$ and it has the form

$$q_f(r,\theta,t)=-C_d\left[\frac{\partial w}{\partial t}+(\Omega-\Omega_d)\frac{\partial w}{\partial \theta}\right], \tag{4}$$

where C_d is a damping coefficient depending on the viscosity of the fluid, the rotational speed of the disk and the geometrical parameters of the enclosure, and Ω_d is the rotational speed of the distributed viscous damping force relative to the disk. Both C_d and Ω_d should be determined by experiments.

The acoustic force $q_a(r,\theta,t)$ on the disk can be calculated through the pressure difference between the upper and lower surfaces of the disk, and can be written as

$$q_a(r,\theta,t)=\rho_a\left[\left.\frac{\partial \phi_a(r,\theta,z,t)}{\partial t}\right|_{z=0^+}-\left.\frac{\partial \phi_a(r,\theta,z,t)}{\partial t}\right|_{z=0^-}\right], \tag{5}$$

in which ϕ_a is the acoustic velocity potential. The governing equation for the acoustic field in the enclosure is expressed by

$$\nabla^2\phi_a=\frac{1}{a^2}\frac{\partial^2\phi_a}{\partial t^2}, \tag{6}$$

where a is the speed of sound in the enclosure, ∇^2 is the space Laplacian operator. The acoustic velocity on the enclosure walls must be zero and the boundary conditions for ϕ_a are

$$\left.\frac{\partial \phi_a}{\partial r}\right|_{r=r_e}=0, \quad \left.\frac{\partial \phi_a}{\partial z}\right|_{z=\pm z_e}=0. \tag{7}$$

In addition, on the surface of the disk, the acoustic velocity should match the disk vibration velocity, and at the clearance between the disk rim and the enclosure, $\phi_a=0$ for the asymmetric acoustic field (Renshaw et al., 1994). So that we have the following conditions:

$$\left.\frac{\partial \phi_a}{\partial z}\right|_{z=0}=\begin{cases}0 & (0\leqslant r<r_i)\\ \dfrac{\partial w}{\partial t} & (r_i\leqslant r\leqslant r_o)\end{cases} \quad \text{and} \quad \left.\phi_a\right|_{z=0}=0, \quad (r_o<r\leqslant r_e). \tag{8}$$

In the following analysis, the variables are normalized by r_o, h, ρ_d, and Ω (Renshaw et al., 1994),

$$\bar{r}=\frac{r}{r_o}, \quad \bar{z}=\frac{z}{r_o}, \quad \bar{t}=\Omega t, \quad \bar{w}=\frac{w}{h}, \quad \kappa=\frac{r_i}{r_o}, \quad \bar{r}_e=\frac{r_e}{r_o}, \quad \bar{z}_e=\frac{z_e}{r_o},$$

$$\bar{\sigma}_r=\frac{\sigma_r}{\rho_d r_o^2\Omega^2}, \quad \bar{\sigma}_\theta=\frac{\sigma_\theta}{\rho_d r_o^2\Omega^2}, \quad \bar{q}_f=\frac{q_f}{\rho_d h^2\Omega^2}, \quad \bar{q}_a=\frac{q_a}{\rho_d h^2\Omega^2} \tag{9}$$

and the nondimensional acoustic velocity and potential are introduced,

$$\bar{\mathbf{v}}_a=\frac{1}{h\Omega}\mathbf{v}_a, \quad \bar{\phi}_a=\frac{\phi_a}{r_o h\Omega}. \tag{10}$$

By using these definitions, all above-mentioned equations can be rewritten in dimensionless form. In order to avoid confusion of the variables, the overbars of the nondimensional variables are omitted in the following analysis. Thus, we have the following equations:

the equation for vibration of the rotating disk

$$\begin{aligned}&\frac{\partial^2 w}{\partial t^2}+2\frac{\partial^2 w}{\partial t\partial\theta}+\frac{\partial^2 w}{\partial\theta^2}+\varepsilon\nabla^4 w-\left[\frac{1}{r}\frac{\partial}{\partial r}\left(r\sigma_r\frac{\partial w}{\partial r}\right)+\frac{1}{r^2}\frac{\partial}{\partial\theta}\left(\sigma_\theta\frac{\partial w}{\partial\theta}\right)\right]\\ &\quad=-C\left[\frac{\partial w}{\partial t}+\left(1-\frac{\Omega_d}{\Omega}\right)\frac{\partial w}{\partial\theta}\right]+\Lambda\left[\frac{\partial\phi_a(r,\theta,z=0^+,t)}{\partial t}-\frac{\partial\phi_a(r,\theta,z=0^-,t)}{\partial t}\right],\end{aligned} \tag{11}$$

and the boundary conditions

$$w|_{r=\kappa}=0, \quad \left.\frac{\partial w}{\partial r}\right|_{r=\kappa}=0, \tag{12}$$

$$\left[\frac{\partial^2 w}{\partial r^2}+\nu\left(\frac{1}{r}\frac{\partial w}{\partial r}+\frac{1}{r^2}\frac{\partial^2 w}{\partial\theta^2}\right)\right]_{r=1}=0,\quad \left[\frac{\partial}{\partial r}(\nabla^2 w)+\frac{(1-\nu)}{r^2}\frac{\partial^2}{\partial\theta^2}\left(\frac{\partial w}{\partial r}-\frac{w}{r}\right)\right]_{r=1}=0. \tag{13}$$

In Eq. (11), $\varepsilon = D/\rho_d r_o^4 h\Omega^2$ is the ratio of the bending stiffness of the disk to the stiffness derived from the centrifugal body force, $C = C_d/\rho_d h\Omega$ is the nondimensional ratio of aerodynamic damping, $\Lambda = \rho_a r_o/\rho_d h$ is the ratio of the densities of the air-flow and the disk (mass ratio). The equation for the acoustic field is

$$\nabla^2\phi_a = M^2\frac{\partial^2\phi_a}{\partial t^2} \tag{14}$$

and the boundary conditions, arising from zero velocity on enclosure walls, are

$$\left.\frac{\partial\phi_a}{\partial r}\right|_{r=r_e}=0,\quad \left.\frac{\partial\phi_a}{\partial z}\right|_{z=\pm z_e}=0, \tag{15}$$

where $M = r_o\Omega/a$ is the Mach number at the outer edge of the disk. The continuity conditions on the disk surface, where the acoustic velocity equals the disk velocity, and at the clearance between the disk rim and the enclosure, where the acoustic pressure is zero, can be written as

$$\left.\frac{\partial\phi_a}{\partial z}\right|_{z=0}=\begin{cases}0 & (0\leqslant r<\kappa)\\ \dfrac{\partial w}{\partial t} & (\kappa\leqslant r\leqslant 1)\end{cases}\quad\text{and}\quad \phi_a|_{z=0}=0,\quad (1<r\leqslant r_e). \tag{16}$$

Eqs. (11) and (14), together with the boundary conditions, form a stability problem for the system of the rotating disk coupled with the air-flow in the enclosure. If the amplitude of the disk vibration, w, grows with time, the system is unstable and flutter occurs.

3. Implementation of the feedback control

In this section, an acoustic feedback control is introduced into the disk-enclosure system. Fig. 2 shows the schematic diagram of the feedback mechanism. A sensor is fixed and placed in the enclosure to pick up the vibration of the disk at a point (r_s, θ_s). The signal is then amplified and phase-shifted to drive the actuator which will generate a surface vibration on the upper surface of the enclosure. This surface vibration is therefore dependent on the control gain G, the phase shift σ, the disk vibration at the sensor point, and the actuator distribution $A(r,\theta)$ on the upper surface. In general, $A(r,\theta)$ can be written as

$$A(r,\theta)=\sum_{n=-\infty}^{\infty} a_n(r)\mathrm{e}^{\mathrm{i}n\theta}. \tag{17}$$

In the feedback control, we only take the nth mode and consider a simple case that $a_n(r)$ is a constant in the actuator region $r\leqslant r_a$ (nondimensionalized by r_o). Due to the motion of the actuator, a controlled acoustic field will be generated in the enclosure, which is denoted as ϕ_c. On the actuating portion, the acoustic velocity induced by ϕ_c equals the actuator velocity, written as $G\mathrm{e}^{\mathrm{i}\sigma}\mathrm{e}^{\mathrm{i}n\theta}\partial w(r_s,\theta_s t)/\partial t$, and on other part of the upper surface, the acoustic velocity is zero. Since the clearance between the disk rim and the sidewall of the enclosure is normally very small, we assume that the gap is negligible and the acoustic velocity induced by ϕ_c on the disk is zero (the acoustic field induced by the disk vibration has been considered in ϕ_a). The equation and the boundary conditions for the controlled acoustic field ϕ_c are

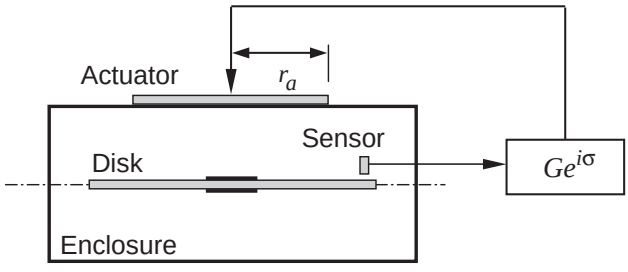

Fig. 2. Schematic diagram of the feedback control.

therefore written as

$$\nabla^2\phi_c = M^2\frac{\partial^2\phi_c}{\partial t^2}, \tag{18}$$

$$\left.\frac{\partial\phi_c}{\partial z}\right|_{z=z_e} = \begin{cases} G\mathrm{e}^{\mathrm{i}\sigma}\mathrm{e}^{\mathrm{i}n\theta}\dfrac{\partial w(r_s,\theta_s,t)}{\partial t} & (r\leqslant r_a),\\ 0 & (r_a<r\leqslant r_e),\end{cases}$$

$$\left.\frac{\partial\phi_c}{\partial z}\right|_{z=0} = 0, \quad \left.\frac{\partial\phi_c}{\partial r}\right|_{r=r_e} = 0. \tag{19}$$

The controlled acoustic field ϕ_c will generate an additional force on the disk surface, denoted by q_c, which can be calculated by

$$q_c = \Lambda\frac{\partial\phi_c(r,\theta,z=0^+,t)}{\partial t}. \tag{20}$$

This control force will be added to the right-hand side of Eq. (11) and the stability of the disk-enclosure system is therefore under the action of control.

4. Method of analysis

In order to solve the air-coupled disk vibration equations, we employ the approximation method used by others (Renshaw et al., 1994; and Hosaka and Crandall, 1992), and assume the transverse displacement $w(r,\theta,t)$ and the acoustic velocity potentials ϕ_a and ϕ_c to have the form

$$w(r,\theta,t) = R(r)\mathrm{e}^{\mathrm{i}(n\theta+\lambda t)}, \tag{21a}$$

$$\phi_a(r,\theta,z,t) = \psi_a(r,z)\mathrm{e}^{\mathrm{i}(n\theta+\lambda t)}, \tag{21b}$$

$$\phi_c(r,\theta,z,t) = \psi_c(r,z)\mathrm{e}^{\mathrm{i}(n\theta+\lambda t)}, \tag{21c}$$

where $R(r)$, $\psi_a(r,z)$ and $\psi_c(r,z)$ are unknown functions to be determined; λ is the eigenvalue whose real part determines the disk vibration frequency and the imaginary part indicates the stability of the system.[2] $R(r)$ is obtained by Galerkin's method in the following form:

$$w(r,\theta,t) = \sum_{m=0}^{\infty} c_m R_{mn}(r)\mathrm{e}^{\mathrm{i}(n\theta+\lambda t)}, \tag{22}$$

where m and n represent the number of nodal circles and number of nodal diameters of the vibration mode (m,n), and c_m are coefficients. In the numerical simulation, the infinite series in Eq. (22) has been truncated at $m=M_0$ within the allowable accuracy and a power series is used to approximate R_{mn} (Chonan et al., 1985):

$$R_{mn}(r) = r^m + r^{m+1} + E_{mn}^{(1)}r^{m+2} + E_{mn}^{(2)}r^{m+3} + r^{m+4} + E_{mn}^{(3)}r^{m+5} + E_{mn}^{(4)}r^{m+6}, \tag{23}$$

where $E_{mn}^{(i)}(i=1,2,3,4)$ are constants to be determined such that all the boundary conditions of the disk are satisfied.

The acoustic velocity potentials ϕ_a and ϕ_c are solved according to the boundary conditions and have the following form:

$$\phi_a(r,\theta,z,t) = \sum_{k=1}^{\infty} d_k^a\cosh[\alpha_k(z_e-z)]\mathrm{J}_n(\xi_k r)\mathrm{e}^{\mathrm{i}(n\theta+\lambda t)}, \tag{24}$$

$$\phi_c(r,\theta,z,t) = \sum_{k=1}^{\infty} d_k^c\cosh(\alpha_k z)\mathrm{J}_n(\xi_k r)\mathrm{e}^{\mathrm{i}(n\theta+\lambda t)}, \tag{25}$$

where $\mathrm{J}_n(\xi_k r)$ is the Bessel function of the nth order, ξ_k is determined by the roots of $\mathrm{J}_n'(\xi_k r_e)=0(k=1,2,\ldots,\infty)$, which is the boundary condition at the sidewall of the enclosure, $\alpha_k = \sqrt{(\xi_k^2 - M^2\lambda^2)}^{1/2}$, d_k^a and d_k^c will be determined, respectively, by the matching condition (16) at $z=0$ and the boundary condition (19) at $z=z_e$.

[2] Thus, the eigenvalues here are what are normally called eigenfrequencies; in the usual nomenclature (not here), it is the real component that defines stability.

For two arbitrary complex-valued functions, $a(r,\theta)$ and $b(r,\theta)$ defined in the domain $\{\kappa \leqslant r \leqslant 1, 0 \leqslant \theta \leqslant 2\pi\}$, we introduce an inner product as follows:

$$\langle a(r,\theta), b(r,\theta)\rangle = \int_0^{2\pi}\int_\kappa^1 a(r,\theta)b^*(r,\theta)r\,\mathrm{d}r\,\mathrm{d}\theta, \tag{26}$$

where the superscript asterisk denotes the complex conjugate. By substituting Eqs. (22), (24) and (25) into the motion Eq. (11) of the disk, and calculating the inner product with $R_{ln}(r)e^{i(n\theta+\lambda t)}, (l=0,1,\ldots,M_0)$, one obtains a matrix equation for the coefficients c_m following Galerkin's method:

$$\{[\mathbf{B}] + [\mathbf{P}^f] + [\mathbf{P}^a] + [\mathbf{P}^c]\}[\mathbf{c}] = [\mathbf{0}], \tag{27}$$

where $[\mathbf{c}] = [\,c_0 \quad c_1 \quad \cdots \quad c_{M_0}\,]^{\mathrm{T}}$, $[\mathbf{B}]$ is a $(M_0+1)\times(M_0+1)$ matrix associated with the free vibration of the rotating disk without any aerodynamic loading, $[\mathbf{P}^f]$ is a $(M_0+1)\times(M_0+1)$ matrix associated with aerodynamic force due to the disk rotation, $[\mathbf{P}^a]$ and $[\mathbf{P}^c]$ are also $(M_0+1)\times(M_0+1)$ matrices and are associated with the acoustic force and the control force, respectively. $[\mathbf{P}^a]$ and $[\mathbf{P}^c]$ are evaluated in Appendix A. The elements for $[\mathbf{B}]$ and $[\mathbf{P}^f]$ are given as follows:

$$B_{ml} = 2\pi\int_\kappa^1 \left[(\lambda+n)^2 R_{mn}(r) - \varepsilon\nabla_n^4 R_{mn}(r) + \frac{1}{r}\left(r\sigma_r\frac{\mathrm{d}R_{mn}}{\mathrm{d}r}\right) - \frac{n^2}{r^2}\sigma_\theta R_{mn}(r)\right] R_{ln}(r)r\,\mathrm{d}r, \tag{28}$$

$$P^f_{ml} = -2\pi\int_\kappa^1 C\mathrm{i}\left[\lambda + \left(1-\frac{\Omega_d}{\Omega}\right)n\right] R_{mn}(r)R_{ln}(r)r\,\mathrm{d}r, \tag{29}$$

where $\nabla_n^4 = \left(\frac{\mathrm{d}^2}{\mathrm{d}r^2} + \frac{\mathrm{d}}{r\mathrm{d}r} - \frac{n^2}{r^2}\right)^2$. In Eq. (27), $[\mathbf{P}^f]$ and $[\mathbf{P}^c]$ are additional terms which were not included in the model of Renshaw et al. (1994). The condition of nontrivial solutions for Eq. (27) leads to a characteristic equation

$$\det\{[\mathbf{B}] + [\mathbf{P}^f] + [\mathbf{P}^a] + [\mathbf{P}^c]\} = 0, \tag{30}$$

from which the eigenvalue λ is obtained from the roots. These roots come in (M_0+1) pairs and generate (M_0+1) pairs of eigenvalues for a fixed nodal diameter n. Each pair of eigenvalues is denoted by λ^{FTW} and λ^{BTW} for the Forward Traveling Wave (FTW) and Backward Traveling Wave (BTW) along and against the rotation direction of the disk [see, e.g., Kim et al. (2000) and Hansen et al. (2001)]. The real parts of the eigenvalues, $\mathscr{R}e(\lambda)$, are related to the disk vibration mode frequencies while the imaginary parts, $\mathscr{I}m(\lambda)$, are related to the 'damping' of the disk vibration, $\mathscr{I}m(\lambda)<0$ indicates an unstable vibration or flutter. If the disk rotates in vacuum, all the eigenvalues are real numbers and the system is therefore stable. If the disk rotates in air without the feedback control, the eigenvalues will be complex numbers and $\mathscr{I}m(\lambda)$ may be negative for some modes, i.e., flutter may occur in these modes. All these cases are demonstrated and discussed in next section.

5. Simulation results and discussions

Case studies are conducted in this section to show that flutter may occur for some modes and that it is possible to suppress flutter by the feedback control technique. The disk used in the simulation is the same one used by D'Angelo and Mote (1993a, b) so that we can compare our results with theirs. The details of the disk are listed in Table 1. In the simulations, the enclosure dimensions are fixed at $z_e = 0.5$ and $r_e = 1.2$, the sensor is located at $(r_s,\theta_s) = (0.9, 0)$ and $r_a = 0.8$.

5.1. Rotating in vacuum (flutter free)

In this case, both aerodynamic loading $[\mathbf{P}^f]$, and acoustic loading $[\mathbf{P}^a]$ and $[\mathbf{P}^c]$ are zero, and the eigenvalues are found to be real numbers. The real parts of the eigenvalues have been converted into the vibration frequencies and the results are plotted in Fig. 3. It is shown that for each mode with $n\neq 0$ the frequency splits as the rotational speed increases from $\Omega=0$, one increases with the rotational speed, which is the FTW, and the other initially decreases to zero and then increases again, which is the BTW. The rotation speeds at which BTW frequencies become zero are called critical speeds.

The critical speed for mode (0, 3) in the present study is 2110 rpm, which is comparable to the 2078 rpm measured by D'Angelo and Mote (1993b), with an error about 1.5%. When the disk is stationary ($\Omega=0$), the FTW and BTW have the same frequency for each mode. The calculated mode frequencies for the stationary disk are compared with the measured results by D'Angelo and Mote (1993a), and the results for some modes are listed in Table 2. The errors are less than 2% for most of modes, except for 5% for modes (0, 0) and (0, 1).

Table 1
Geometric and material parameters of the disk

Parameter	Value
Young's modulus, E	200(GPa)
Density of disk, ρ_d	7.8×10^3(kg/m^3)
Outer radius, r_o	0.178 (m)
Clamping ratio, κ	0.3
Thickness, h	0.775(mm)
Density of air, ρ_a	1.21(kg/m^3)
Speed of sound in air, a	340 (m/s)

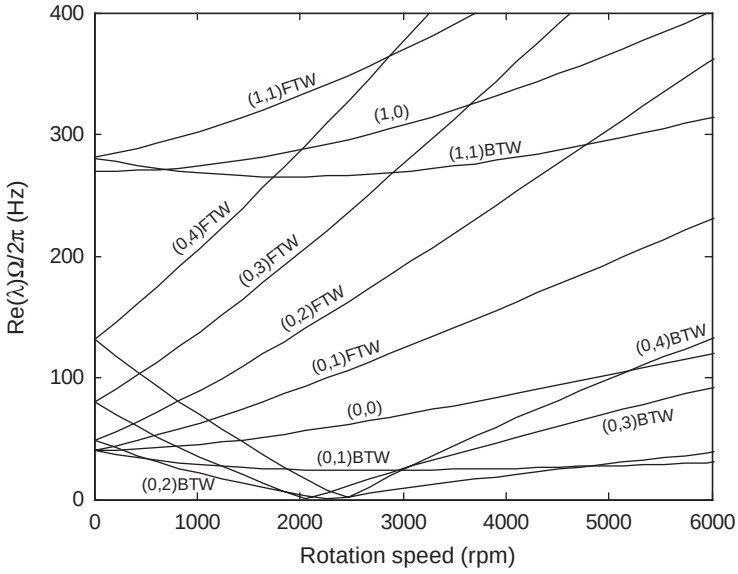

Fig. 3. Mode frequency versus rotation speed of the disk in vacuum.

5.2. Rotating in air (flutter observation)

In this case, we take into account the aerodynamic loading [$\mathbf{P}^f$] and [$\mathbf{P}^a$], but keep the control term zero. As we mentioned earlier, the aerodynamic loading [Eq. (4)] is an empirical model, the nondimensional parameter C and speed ratio Ω_d/Ω in Eq. (11) should be determined according to experimental data, such as the disk flutter speed. Our simulation indicates that the flutter speed is not sensitive to the damping coefficient in a range of $0.005 < C < 0.05$, so that we set $C = 0.01$ by considering that the aerodynamic loading is a kind of 'damping' before onset of flutter and it should be light comparing to the disk material damping, which is in order of 0.01–0.1 (Jones, 2000).

We conducted an experiment to measure the flutter speed on two different disks (the results will be reported in another paper) and found that the speed ratio Ω_d/Ω in the model should be in a range of 0.8–0.86 in order to have the predicted flutter speeds agree with measured values.

In the present study, we set $\Omega_d/\Omega = 0.8$ and find that predicted flutter mode and speed are very close to the observed value, which will be shown later. The real parts and the imaginary parts of the eigenvalues have been converted into mode frequencies and mode dampings, respectively, and the results are plotted versus rotational speed in Fig. 4. The mode frequencies showing in Fig. 4(a) are similar to those in Fig. 3, consisting of FTWs and BTWs, except that the aerodynamic loading has reduced natural frequencies by less than 1%, shown in Table 2. The imaginary parts of the eigenvalues, which are shown in Fig. 4(b), are not zero due to the aerodynamic loading. It is seen that damping for BWT modes (0, 3), (0, 4) and (0, 5) are initially positive, but become negative as the rotation speed increases, indicating that the rotating disk is unstable or flutter occurs above these speeds. The speed at which the damping changes from positive to negative is denoted as the flutter speed. Fig. 4(b) shows that flutter occurs first in mode (0, 3), which agrees

Table 2
Natural frequency of a stationary disk

Mode	Experiment (Hz) disk in vacuum (D'Angelo and Mote, 1993a)	Calculation (Hz) disk in vacuum	Calculation (Hz) disk in air
(0, 0)	38.40±0.24	40.69	40.46
(0, 1)	37.19±0.29	40.31	39.98
(0, 2)	47.10±0.49	48.83	48.52
(0, 3)	79.78±0.90	79.94	79.53
(0, 4)	133.08±1.04	131.81	131.23
(0, 5)	202.18±1.02	199.95	199.19

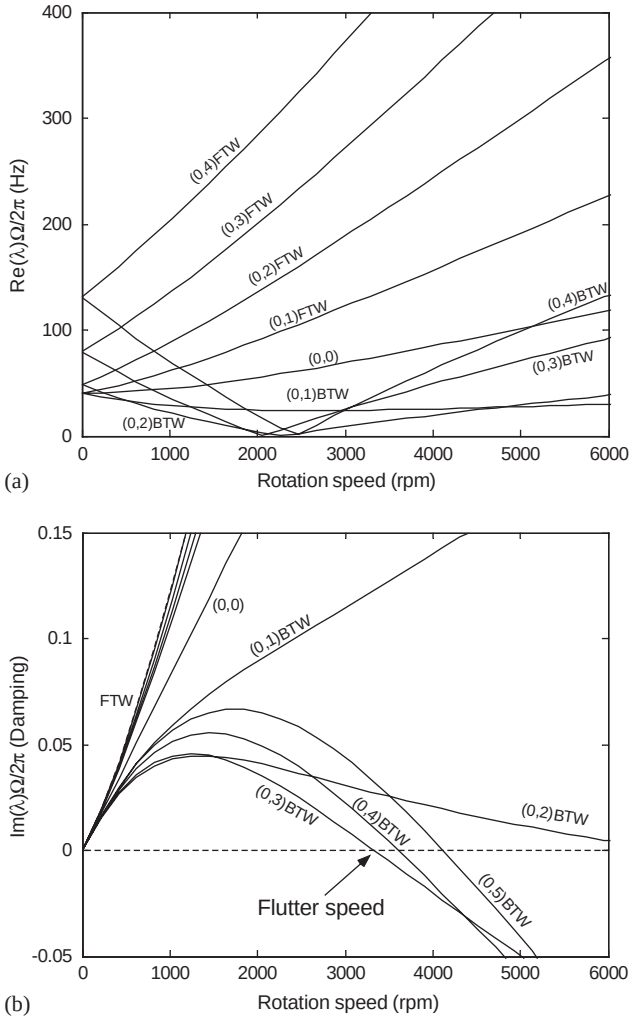

Fig. 4. The disk in the enclosure with air-coupling. (a) Mode frequency versus rotation speed. (b) Imaginary part of the eigenvalues versus rotation speed for some modes.

with the observation by D'Angelo and Mote (1993b). The flutter speed corresponding to the (0, 3) mode is found to be 3200 rpm in the present model, which is close to 3500 rpm reported by D'Angelo and Mote (1993b). It should be pointed out that the accuracy of flutter prediction depends on the model of the aerodynamic loading on the disk, which is another research topic involving the aerodynamics of the flow around the rotating disk and the disk-air coupling. The

present study focuses on whether flutter can be suppressed by the feedback control technique, and this will be discussed next.

5.3. Performance of the feedback control

The feedback control is actuated by adding the control term $[\mathbf{P}^c]$ in Eq. (30), and the control performance is evaluated based on the effect of the control on the imaginary parts of the eigenvalues. It is seen from Fig. 5 that the damping curves are lifted up by the control for modes (0, 3) and (0, 4) when the phase shift is set at $\sigma = \pi/2$. In other words, the flutter speeds for these modes have been increased with the feedback control, and the stability of the rotating disk is therefore improved. How much the stability can be improved depends on the control gain. At the correct phase shift (e.g. $\sigma = \pi/2$), the greater the gain is, the more stable the disk will be. It is shown in Fig. 5(a) that, for mode (0, 3), the control has increased the flutter speed to 4000 rpm with $G = 8$ and brought the whole damping curve above zero if $G > 16$. On the other hand, it is also illustrated in Fig. 5 that feedback control may make the disk more unstable by increasing the 'damping' if the phase shift is set at $\sigma = -\pi/2$, showing that the performance of the control scheme is very much dependent on both the gain and phase shift.

The control-induced damping can be viewed by subtracting $\mathcal{I}m[\lambda(G = 0)]$ from $\mathcal{I}m[\lambda(G \neq 0)]$, and this is shown in Fig. 6 for mode (0, 3). It is seen that the control induced damping decreases with the rotation speed to zero at the critical

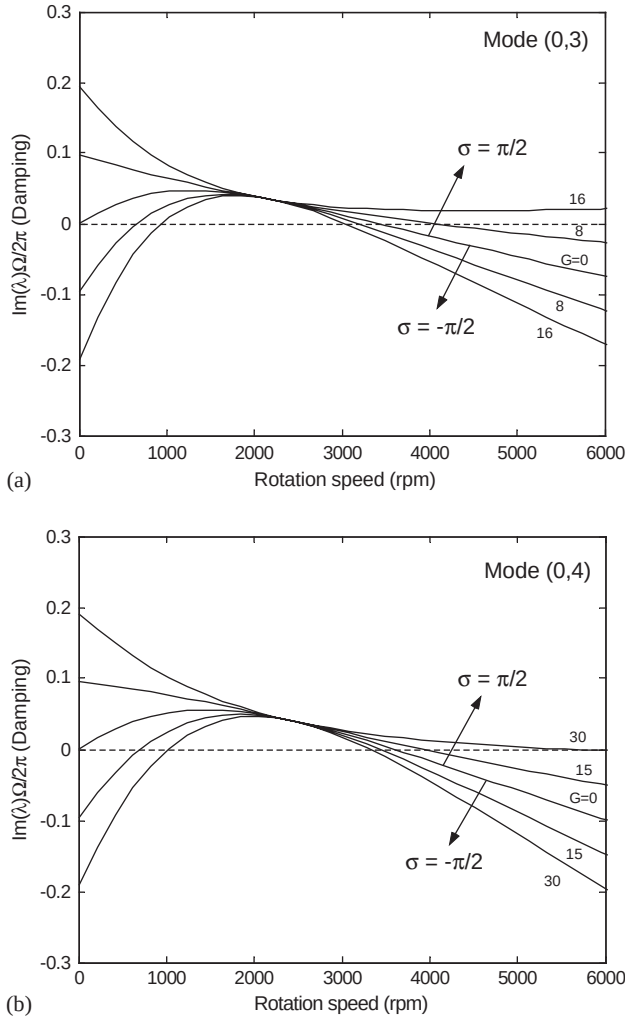

Fig. 5. The effect of control on $\mathcal{I}m(\lambda)$ with different phase shift and gain for modes (0, 3) and (0, 4).

speed, and then increases, almost linearly with the rotation speed. This is the same as the variation of the mode frequency with the rotation speed for BTWs, and we deduce that the control damping is proportional to the mode frequency observed in the fixed coordinates.

Fig. 7 is a 3-D plot to show variation of the aerodynamic damping with the control gain G and phase shift σ and Fig. 8 is a stability map in the σ–G plane. The stability map consists of a stable region, in which $\mathscr{I}m(\lambda)<0$, and an unstable region, in which $\mathscr{I}m(\lambda)>0$. The boundary between the stable region and the unstable region, at which $\mathscr{I}m(\lambda)=0$, depends on the rotation speed. Figs. 7 and 8 show that the control is robust because it works in a region with different combinations of G and σ, rather than at a point. The results for other higher modes are very similar to those presented here for mode (0, 3).

It may be interesting and beneficial to mention the control mechanism in feedback control of disk flutter. In fact, the aerodynamics involved in coupling between the air and rotating disk is quite complicated, which is the reason why there are no theoretical models for the aerodynamic loading term, but only empirical ones. However, since flutter is a kind of aeroelastic instability, in which aerodynamic energy is supplied to the disk structure through the coupling at a rate faster than it is dissipated, it is reasonable to suggest that the feedback control in this case may weaken the air-disk

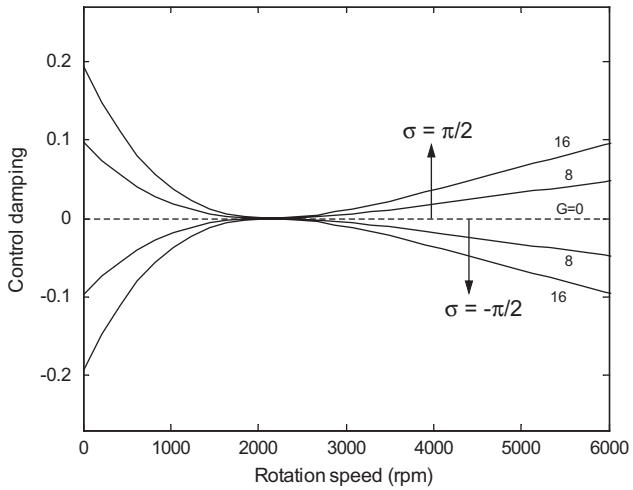

Fig. 6. The control-induced 'damping' $\mathscr{I}m[\lambda G\neq 0)] - \mathscr{I}m[\lambda G = 0)]$ versus rotation speed for mode (0, 3).

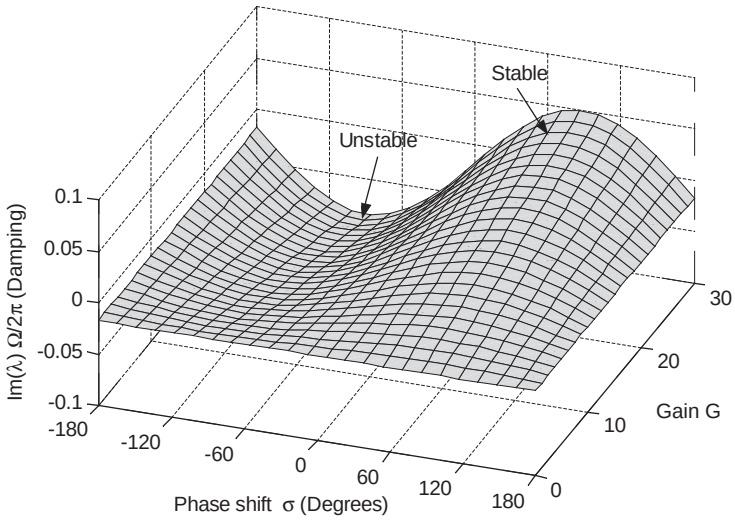

Fig. 7. A 3-D diagram to show the control effect on $\mathscr{I}m(\lambda)$ for mode (0, 3). The rotation speed is set at $\Omega=4000$ rpm.

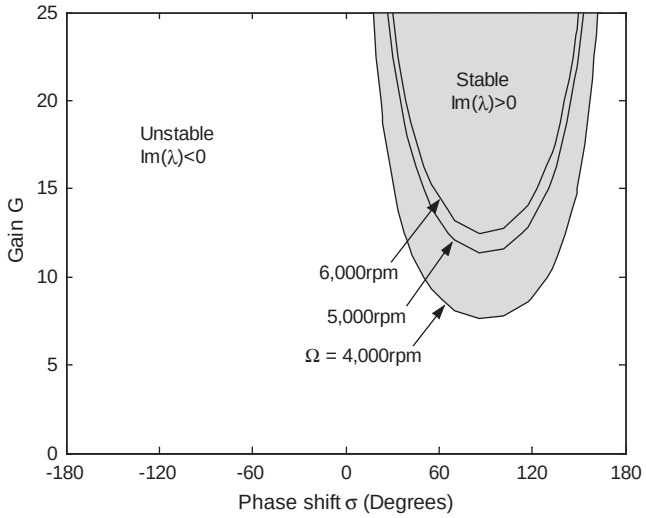

Fig. 8. Stability map to show the control performance for mode (0, 3).

coupling so as to prevent the energy from being supplied into the disk structure. It would be helpful to view the disk with the feedback control as a complete dynamical system which is more stable than the original one without control.

6. Conclusions

A feedback control technique is proposed to suppress the flutter of a rotating disk in an enclosure. The stability of the disk-enclosure system, together with the feedback control, has been studied by calculating the eigenvalues for the disk modes. It is shown that the rotating disk is strongly coupled with both the flow field spinning around the disk and the acoustic field induced by the disk vibrations. Disk flutter is observed for some modes when the rotation speed is above certain values. The present model predicts that the flutter occurs first in (0.3) mode at speed 3200 rpm, which agrees reasonably well with the observation in experiments by D'Angelo and Mote (1993b). It is demonstrated that the controller, which generates a controlled acoustic pressure inside the enclosure, can effectively suppress disk flutter by changing the imaginary part of the eigenvalues of the disk-enclosure system from negative to positive at a given rotation speed, and the controller has a large operation range in terms of the selection of the gain and the phase shift. It is hoped that this study may provide an option to control disk flutter.

Acknowledgements

The authors would like to acknowledge the finance support provided by Agency for Science, Technology & Research of Singapore and Center for Mechanics of Micro-Systems, Nanyang Technological University.

Appendix A

The application of the inner product on Eq. (11) (including the control force q_c) with $R_{ln}(r)e^{i(n\theta+\lambda t)}, (l = 0, 1, \ldots, M_0)$ generates an acoustic force vector $[\boldsymbol{q}^a]$ and a control force vector $[\boldsymbol{q}^c]$ on the right-hand side. The elements for $[\boldsymbol{q}^a]$ and $[\boldsymbol{q}^c]$ are, respectively,

$$q_l^a = \int_0^{2\pi}\int_\kappa^1 \Lambda\left(\frac{\partial\phi_a(r,\theta,z=0^+,t)}{\partial t} - \frac{\partial\phi_a(r,\theta,z=0^-,t)}{\partial t}R_{ln}(r)e^{-i(n\theta+\lambda t)}r\,dr\,d\theta\right)$$
$$= 4\pi\int_\kappa^1 \Lambda\lambda i\left[\sum_{k=1}^{\infty} d_k^a \cosh(\alpha_k z_e)J_n(\xi_k r)\right]R_{ln}(r)r\,dr, \tag{A.1}$$

$$q_l^c = \int_0^{2\pi}\int_\kappa^1 \Lambda\frac{\partial\phi_c(r,\theta,z=0^+,t)}{\partial t}R_{ln}(r)\mathrm{e}^{-\mathrm{i}(n\theta+\lambda t)}r\,\mathrm{d}r\,\mathrm{d}\theta$$
$$= 2\pi\int_\kappa^1 \Lambda\lambda i\left[\sum_{k=1}^{\infty} d_k^c \mathrm{J}_n(\xi_k r)\right]R_{ln}(r)r\,\mathrm{d}r. \tag{A.2}$$

The infinite series in the integrals are truncated at $k=K_0$, and we introduce the following vectors

$$[\mathbf{Y}] = [\,R_{0n}(r) \quad R_{1n}(r) \quad \cdots \quad R_{M_0n}(r)\,]^{\mathrm{T}}, \tag{A.3}$$

$$[\Phi^a] = [\,\cosh(\alpha_1 z_e)\mathrm{J}_n(\xi_1 r) \quad \cosh(\alpha_2 z_e)\mathrm{J}_n(\xi_2 r) \quad \cdots \quad \cosh(\alpha_{K_0} z_e)\mathrm{J}_n(\xi_{K_0} r)\,], \tag{A.4}$$

$$[\Phi^c] = [\,\mathrm{J}_n(\xi_1 r) \quad \mathrm{J}_n(\xi_2 r) \quad \cdots \quad \mathrm{J}_n(\xi_{K_0} r)\,], \tag{A.5}$$

$$[\mathbf{D}^a] = [\,d_1^a \quad d_2^a \quad \cdots \quad d_{K_0}^a\,]^{\mathrm{T}}, \tag{A.6}$$

$$[\mathbf{D}^c] = [\,d_1^c \quad d_2^c \quad \cdots \quad d_{K_0}^c\,]^{\mathrm{T}} \tag{A.7}$$

and rewrite $[\boldsymbol{q}^a]$ and $[\boldsymbol{q}^c]$ in the following form:

$$[\boldsymbol{q}^a] = 4\pi\Lambda\lambda\mathrm{i}\int_\kappa^1 \{[\mathbf{Y}][\Phi^a][\mathbf{D}^a]\}r\,\mathrm{d}r, \tag{A.8}$$

$$[\boldsymbol{q}^c] = 2\pi\Lambda\lambda\mathrm{i}\int_\kappa^1 \{[\mathbf{Y}][\Phi^c][\mathbf{D}^c]\}r\,\mathrm{d}r. \tag{A.9}$$

Both $[\mathbf{D}^a]$ and $[\mathbf{D}^c]$ are related to the disk vibrations, i.e. $[\mathbf{c}]$, through the boundary conditions, and we give a detailed derivation on an explicit form for $[\mathbf{D}^a]$. Substituting Eqs. (24) and (22) into the continuity conditions (16), we have

$$\sum_{k=1}^{\infty} d_k^a\alpha_k\sinh(\alpha_k z_e)\mathrm{J}_n(\xi_k r) = 0, \quad \text{at } 0\leqslant r<\kappa, \tag{A.10}$$

$$-\sum_{k=1}^{\infty} d_k^a\alpha_k\sinh(\alpha_k z_e)\mathrm{J}_n(\xi_k r) = \sum_{m=0}^{M_0} c_m\lambda\mathrm{i}R_{mn}(r), \quad \text{at } \kappa\leqslant r\leqslant 1, \tag{A.11}$$

$$\sum_{k=1}^{\infty} d_k^a\cosh(\alpha_k z_e)\mathrm{J}_n(\xi_k r) = 0, \quad \text{at } 1<r\leqslant r_e. \tag{A.12}$$

We take the finite terms of $k=1,2,3,\ldots,K_0$ for the truncation of the infinite series in Eqs. (A.10)–(A.12) and choose finite points $r=r_j (j=1,2,3,\ldots,K_0)$ in the domain of $0\leqslant r\leqslant r_e$ for approximate satisfaction of Eqs. (A.10)–(A.12). This leads to a set of equations

$$\begin{bmatrix}
\alpha_1\sinh(\alpha_1 z_e)\mathrm{J}_n(\xi_1 r_1) & \alpha_2\sinh(\alpha_2 z_e)\mathrm{J}_n(\xi_2 r_1) & \cdots & \alpha_{K_0}\sinh(\alpha_{K_0} z_e)\mathrm{J}_n(\xi_{K_0} r_1)\\
\alpha_1\sinh(\alpha_1 z_e)\mathrm{J}_n(\xi_1 r_2) & \alpha_2\sinh(\alpha_2 z_e)\mathrm{J}_n(\xi_2 r_2) & \cdots & \alpha_{K_0}\sinh(\alpha_{K_0} z_e)\mathrm{J}_n(\xi_{K_0} r_2)\\
\vdots & \vdots & \ddots & \vdots\\
\alpha_1\sinh(\alpha_1 z_e)\mathrm{J}_n(\xi_1 r_{K_0^1}) & \alpha_2\sinh(\alpha_2 z_e)\mathrm{J}_n(\xi_2 r_{K_0^1}) & \cdots & \alpha_{K_0}\sinh(\alpha_{K_0} z_e)\mathrm{J}_n(\xi_{K_0} r_{K_0^1})\\
-\alpha_1\sinh(\alpha_1 z_e)\mathrm{J}_n(\xi_1 r_{K_0^1+1}) & -\alpha_2\sinh(\alpha_2 z_e)\mathrm{J}_n(\xi_2 r_{K_0^1+1}) & \cdots & -\alpha_{K_0}\sinh(\alpha_{K_0} z_e)\mathrm{J}_n(\xi_{K_0} r_{K_0^1+1})\\
\vdots & \vdots & \ddots & \vdots\\
-\alpha_1\sinh(\alpha_1 z_e)\mathrm{J}_n(\xi_1 r_{K_0^1+K_0^2}) & -\alpha_2\sinh(\alpha_2 z_e)\mathrm{J}_n(\xi_2 r_{K_0^1+K_0^2}) & \cdots & -\alpha_{K_0}\sinh(\alpha_{K_0} z_e)\mathrm{J}_n(\xi_{K_0} r_{K_0^1+K_0^2})\\
\cosh(\alpha_1 z_e)\mathrm{J}_n(\xi_1 r_{K_0^1+K_0^2+1}) & \cosh(\alpha_2 z_e)\mathrm{J}_n(\xi_2 r_{K_0^1+K_0^2+1}) & \cdots & \cosh(\alpha_{K_0} z_e)\mathrm{J}_n(\xi_{K_0} r_{K_0^1+K_0^2+1})\\
\vdots & \vdots & \ddots & \vdots\\
\cosh(\alpha_1 z_e)\mathrm{J}_n(\xi_1 r_{K_0}) & \cosh(\alpha_2 z_e)\mathrm{J}_n(\xi_2 r_{K_0}) & \cdots & \cosh(\alpha_{K_0} z_e)\mathrm{J}_n(\xi_{K_0} r_{K_0})
\end{bmatrix}$$

$$\times \begin{bmatrix} d_1^a \\ d_2^a \\ \vdots \\ d_{K_0^1}^a \\ d_{K_0^1+1}^a \\ \vdots \\ d_{K_0^1+K_0^2}^a \\ d_{K_0^1+K_0^2+1}^a \\ \vdots \\ d_{K_0}^a \end{bmatrix} = \begin{bmatrix} 0 \\ 0 \\ \vdots \\ 0 \\ \sum_{m=0}^{M_0} c_m \lambda \mathrm{i} R_{mn}(r_{K_0^1+1}) \\ \vdots \\ \sum_{m=0}^{M_0} c_m \lambda \mathrm{i} R_{mn}(r_{K_0^1+K_0^2}) \\ 0 \\ \vdots \\ 0 \end{bmatrix}, \tag{A.13}$$

where K_0^1, K_0^2 and $K_0 - K_0^1 - K_0^2$ are the numbers of the chosen points in $0 \leqslant r_j < \kappa$, $\kappa \leqslant r_j \leqslant 1$, and $1 < r_j \leqslant r_e$, respectively. Eq. (A.13) can be written in a matrix form:

$$[\mathbf{A}^a][\mathbf{D}^a] = \mathrm{i}\lambda[\mathbf{R}^a][\mathbf{c}], \tag{A.14}$$

in which, $[\mathbf{A}^a]$ is a $K_0 \times K_0$ matrix

$$[\mathbf{A}^a] = \begin{bmatrix} \alpha_1 \sinh(\alpha_1 z_e)\mathrm{J}_n(\xi_1 r_1) & \alpha_2 \sinh(\alpha_2 z_e)\mathrm{J}_n(\xi_2 r_1) & \cdots & \alpha_{K_0} \sinh(\alpha_{K_0} z_e)\mathrm{J}_n(\xi_{K_0} r_1) \\ \alpha_1 \sinh(\alpha_1 z_e)\mathrm{J}_n(\xi_1 r_2) & \alpha_2 \sinh(\alpha_2 z_e)\mathrm{J}_n(\xi_2 r_2) & \cdots & \alpha_{K_0} \sinh(\alpha_{K_0} z_e)\mathrm{J}_n(\xi_{K_0} r_2) \\ \vdots & \vdots & \ddots & \vdots \\ \alpha_1 \sinh(\alpha_1 z_e)\mathrm{J}_n(\xi_1 r_{K_0^1}) & \alpha_2 \sinh(\alpha_2 z_e)\mathrm{J}_n(\xi_2 r_{K_0^1}) & \cdots & \alpha_{K_0} \sinh(\alpha_{K_0} z_e)\mathrm{J}_n(\xi_{K_0} r_{K_0^1}) \\ -\alpha_1 \sinh(\alpha_1 z_e)\mathrm{J}_n(\xi_1 r_{K_0^1+1}) & -\alpha_2 \sinh(\alpha_2 z_e)\mathrm{J}_n(\xi_2 r_{K_0^1+1}) & \cdots & -\alpha_{K_0} \sinh(\alpha_{K_0} z_e)\mathrm{J}_n(\xi_{K_0} r_{K_0^1+1}) \\ \vdots & \vdots & \ddots & \vdots \\ -\alpha_1 \sinh(\alpha_1 z_e)\mathrm{J}_n(\xi_1 r_{K_0^1+K_0^2}) & -\alpha_2 \sinh(\alpha_2 z_e)\mathrm{J}_n(\xi_2 r_{K_0^1+K_0^2}) & \cdots & -\alpha_{K_0} \sinh(\alpha_{K_0} z_e)\mathrm{J}_n(\xi_{K_0} r_{K_0^1+K_0^2}) \\ \cosh(\alpha_1 z_e)\mathrm{J}_n(\xi_1 r_{K_0^1+K_0^2+1}) & \cosh(\alpha_2 z_e)\mathrm{J}_n(\xi_2 r_{K_0^1+K_0^2+1}) & \cdots & \cosh(\alpha_{K_0} z_e)\mathrm{J}_n(\xi_{K_0} r_{K_0^1+K_0^2+1}) \\ \vdots & \vdots & \ddots & \vdots \\ \cosh(\alpha_1 z_e)\mathrm{J}_n(\xi_1 r_{K_0}) & \cosh(\alpha_2 z_e)\mathrm{J}_n(\xi_2 r_{K_0}) & \cdots & \cosh(\alpha_{K_0} z_e)\mathrm{J}_n(\xi_{K_0} r_{K_0}) \end{bmatrix}$$

and $[\mathbf{R}^a]$ is a $K_0 \times (M_0 + 1)$ matrix

$$[\mathbf{R}^a] = \begin{bmatrix} 0 & & & \\ \vdots & & & \\ 0 & & & \\ R_{0n}(r_{K_0^1+1}) & R_{1n}(r_{K_0^1+1}) & \cdots & R_{M_0 n}(r_{K_0^1+1}) \\ R_{0n}(r_{K_0^1+2}) & R_{1n}(r_{K_0^1+2}) & \cdots & R_{M_0 n}(r_{K_0^1+2}) \\ \vdots & \vdots & \vdots & \vdots \\ R_{0n}(r_{K_0^1+K_0^2}) & R_{1n}(r_{K_0^1+K_0^2}) & \cdots & R_{M_0 n}(r_{K_0^1+K_0^2}) \\ 0 & & & \\ \vdots & & & \\ 0 & & & \end{bmatrix}. \tag{A.15}$$

From Eq. (A.14) we obtain

$$[\mathbf{D}^a] = \mathrm{i}\lambda[\mathbf{A}^a]^{-1}[\mathbf{R}^a][\mathbf{c}] \tag{A.16}$$

and substituting (A.16) into (A.8) yields

$$\begin{aligned} [\boldsymbol{q}^a] &= -4\pi\Lambda\lambda^2 \int_\kappa^1 \{[\mathbf{Y}][\Phi^a][\mathbf{A}^a]^{-1}[\mathbf{R}^a][\mathbf{c}]\} r \,\mathrm{d}r \\ &= \left[-4\pi\Lambda\lambda^2 \int_\kappa^1 \{[\mathbf{Y}][\Phi^a][\mathbf{A}^a]^{-1}[\mathbf{R}^a]\} r \,\mathrm{d}r\right][\mathbf{c}] = [\mathbf{P}^a][\mathbf{c}], \end{aligned} \tag{A.17}$$

where

$$[\mathbf{P}^a] = -4\pi\Lambda\lambda^2 \int_\kappa^1 \{[\mathbf{Y}][\Phi^a][\mathbf{A}^a]^{-1}[\mathbf{R}^a]\} r \, \mathrm{d}r. \tag{A.18}$$

A similar procedure can be applied to $[q^c]$ to get

$$[\mathbf{D}^c] = \mathrm{i}\lambda G \mathrm{e}^{\mathrm{i}\sigma} \mathrm{e}^{\mathrm{i}n\theta_s} [\mathbf{A}^c]^{-1}[\mathbf{R}^c][\mathbf{c}], \tag{A.19}$$

the matrix associated with the control force

$$[\mathbf{P}^c] = -2\pi\Lambda\lambda^2 G \mathrm{e}^{\mathrm{i}\sigma} \mathrm{e}^{\mathrm{i}n\theta_s} \int_\kappa^1 \{[\mathbf{Y}][\Phi^c][\mathbf{A}^c]^{-1}[\mathbf{R}^c]\} r \, \mathrm{d}r. \tag{A.20}$$

In Eqs. (A.19) and (A.20),

$$[\mathbf{A}^c] = \begin{bmatrix} \alpha_1 \sinh(\alpha_1 z_e) \mathrm{J}_n(\xi_1 r_1) & \alpha_2 \sinh(\alpha_2 z_e) \mathrm{J}_n(\xi_2 r_1) & \cdots & \alpha_{K_0} \sinh(\alpha_{K_0} z_e) \mathrm{J}_n(\xi_{K_0} r_1) \\ \alpha_1 \sinh(\alpha_1 z_e) \mathrm{J}_n(\xi_1 r_2) & \alpha_2 \sinh(\alpha_2 z_e) \mathrm{J}_n(\xi_2 r_2) & \cdots & \alpha_{K_0} \sinh(\alpha_{K_0} z_e) \mathrm{J}_n(\xi_{K_0} r_2) \\ \vdots & \vdots & \ddots & \vdots \\ \alpha_1 \sinh(\alpha_1 z_e) \mathrm{J}_n(\xi_1 r_{K_0^a}) & \alpha_2 \sinh(\alpha_2 z_e) \mathrm{J}_n(\xi_2 r_{K_0^a}) & \cdots & \alpha_{K_0} \sinh(\alpha_{K_0} z_e) \mathrm{J}_n(\xi_{K_0} r_{K_0^a}) \\ \alpha_1 \sinh(\alpha_1 z_e) \mathrm{J}_n(\xi_1 r_{K_0^a+1}) & \alpha_2 \sinh(\alpha_2 z_e) \mathrm{J}_n(\xi_2 r_{K_0^a+1}) & \cdots & \alpha_{K_0} \sinh(\alpha_{K_0} z_e) \mathrm{J}_n(\xi_{K_0} r_{K_0^a+1}) \\ \vdots & \vdots & \ddots & \vdots \\ \alpha_1 \sinh(\alpha_1 z_e) \mathrm{J}_n(\xi_1 r_{K_0}) & \alpha_2 \sinh(\alpha_2 z_e) \mathrm{J}_n(\xi_2 r_{K_0}) & \cdots & \alpha_{K_0} \sinh(\alpha_{K_0} z_e) \mathrm{J}_n(\xi_{K_0} r_{K_0}) \end{bmatrix},$$

$$[\mathbf{R}^c] = \begin{bmatrix} R_{0n}(r_s) & R_{1n}(r_s) & \cdots & R_{M_0 n}(r_s) \\ \vdots & \vdots & \ddots & \vdots \\ R_{0n}(r_s) & R_{1n}(r_s) & \cdots & R_{M_0 n}(r_s) \\ & 0 & & \\ & \vdots & & \\ & 0 & & \end{bmatrix},$$

in which K_0^a, $K_0 - K_0^a$ are the numbers of the chosen points in $r_j \leqslant r_a$ and $r_a < r_j \leqslant r_e$ on the upper surface of enclosure, respectively.

References

Chonan, S., Mikami, T., Ishikawa, H., 1985. The vibration and critical speeds of rotating sawblades. Proceedings of JSME, Part C (in Japanese) 52, 1805–1812.

Chonan, S., Jiang, Z.W., Shyu, Y.J., 1992. Stability analysis of a 2″ floppy disk drive system and the optimum design of the disk stabilizer. Journal of Vibration and Acoustics 114, 283–286.

D'Angelo, C., Mote Jr., C.D., 1993a. Natural frequencies of a thin disk, clamped by thick collars with friction at the contacting surfaces, spinning at high rotation speed. Journal of Sound and Vibration 168, 1–14.

D'Angelo, C., Mote Jr., C.D., 1993b. Aerodynamically excited vibration and flutter of a thin disk rotating at supercritical speed. Journal of Sound and Vibration 168, 15–30.

Hansen, M.H., Raman, A., Mote Jr., C.D., 2001. Estimation of nonconservative aerodynamic pressure leading to flutter of spinning disks. Journal of Fluids and Structures 15, 39–57.

Heckl, Maria, A., Huang, X.Y., 2000. Curve squeal of train wheels—part 3, active control. Journal of Sound and Vibration 229, 709–735.

Hosaka, H., Crandall, S., 1992. Self-excited vibrations of a flexible disk rotating on an air film above a flat surface. Acta Mechanica 3, 115–127.

Huang, F., Mote Jr., C.D., 1995. On the instability mechanism of a disk rotating close to a rigid surface. Journal of Applied Mechanics 62, 764–771.

Huang, X.Y., 1987. Active control of aerofoil flutter. Journal of AIAA 25, 1126–1131.

Huang, X.Y., Weaver, D.S., 1991. On the active control of shear layer oscillations across a cavity in the presence of pipeline acoustic resonance. Journal of Fluids and Structures 207–219.

Jones, D.G., 2000. Handbook of Viscoelastic Vibration Damping. Wiley, New York.

Kim, B.C., Raman, A., Mote Jr., C.D., 2000. Prediction of aeroelastic flutter in a hard disk drive. Journal of Sound and Vibration 238, 309–325.

Renshaw, A.A., 1998. Critical speeds for floppy disks. Journal of Applied Mechanics 65, 116–120.

Renshaw, A.A., D'Angelo, C., Mote Jr., C.D., 1994. Aerodynamically excited vibration of a rotating disk. Journal of Sound and Vibration 177, 577–590.

Yasuda, K., Torii, T., Shimizu, T., 1992. Self-excited oscillations of a circular disk rotating in air. JSME International Journal, Series III, 35, 347–352.